Geometric and Exotic Contextuality in Quantum Reality

Michel Planat

1 Introduction

What is quantum reality? Quoting Niels Bohr: *We are suspended in language in such a way that we cannot say what is up and what is down. The world "reality" is also a word, a word which we must learn to use correctly* (Bohr, 1997). Today, the words 'quantum holism' are often used to qualify the inseparability of distant quantum objects known as quantum entanglement or quantum non-locality (Esfeld, 1999; Ferrero et al., 2004; Miller, 2014). The concept of 'quantum contextuality' seems to be more appropriate because it is used to describe our objective experience of quantum measurements. In a contextual world, the measured value of an observable depends on which other mutually compatible measurements might be performed and cannot simply be thought as revealing a pre-existing value. It is not only that the whole supersedes the parts but that the observer interprets the quantum world with his available sensors and words. Quantum contextuality is able to feature counter-intuitive aspects of the quantum language and is now considered as more general than quantum entanglement and quantum non-locality (at least when one refers to Bell's theorem).

In this line of thought, the Bell-Kochen-Specker theorem (BKS) is able to rule out non-contextual hidden variable theories by resorting to mathematical statements about coloring of rays located on maximal orthonormal bases in a d-dimensional Hilbert space (with d at least 3) (Peres, 1993; Quantum contextuality, 2021). A very transparent 'proof' of the BKS theorem makes use of 18 rays and 9 maximal orthonormal bases of two qubits (i.e. in the 4-dimensional Hilbert space) (Cabello et al., 1996). This topic will be described in some details in Sect. 2.

In the past few years, the author developed a group theoretical approach of quantum contextuality that he called 'geometric contextuality'. The idea is to take seri-

M. Planat (✉)
Université de Bourgogne/Franche-Comté, Institut FEMTO-ST CNRS UMR 6174, 15 B Avenue des Montboucons, 25044 Besançon, France
e-mail: michel.planat@femto-st.fr

S. Wuppuluri and I. Stewart (eds.), *From Electrons to Elephants and Elections*,
The Frontiers Collection, https://doi.org/10.1007/978-3-030-92192-7_26

ously Bohr's suggestion that quantum theory is a language. Most of the time, words in this language only need two letters and the theory resorts to the so-called 'dessins d'enfants' of Grothendieck (Planat, 2015, 2016; Planat and Zainuddin, 2017). This topic is developed in Sect. 3 by restricting to the case of two qubits in order to keep the technicalities simple enough.

Then, in Sect 4, the topic 'exotic contextuality' offers an opportunity to reintroduce a four-dimensional space-time in our interpretation of the quantum world. Our objects are four-manifolds. Quantum measurements may be seen as taking place in 'parallel' worlds/contexts that mathematically are homeomorphic but non diffeomorphic to each other (Planat, 2020). This idea looks like the many worlds interpretation of quantum mechanics (DeWitt, 1970) while being different in the mathematical approach.

2 A Glance at Two-Qubit Parity Proofs of the BKS Theorem

A parity proof of BKS theorem is a set of v rays that form l bases (l odd) such that each ray occurs an even number of times over these bases. A proof of BKS theorem is critical if it cannot be further simplified by deleting even a single ray or a single basis. The smallest BKS proof in dimension 4 is a parity proof and corresponds to arrangements of real observables arising from the two-qubit Pauli group, more specifically as eigenstates of two-qubit operators forming a (3×3)-grid (also known as a Mermin's square) as follows

$$\begin{array}{ccc} | & | & || \\ IX- & XI- & XX- \\ | & | & || \\ ZX- & XZ- & YY- \\ | & | & || \\ ZI- & IZ- & ZZ- \\ | & | & || \end{array} \tag{1}$$

where I is the two-dimensional identity matrix, X, Y and Z are the Pauli spin matrices, and the operator products are Kronecker products.

The simplification of arguments in favour of a contextual view of quantum measurements started with Peres' note (1993) and Mermin's report (1993). Observe that in (1), the three operators in each row and each column mutually commute and their product is the identity matrix, except for the right hand side column whose product is minus the identity matrix. There is no way of assigning multiplicative properties to the eigenvalues ± 1 of the nine operators while still keeping the same multiplicative properties for the operators. Paraphrasing (Peres, 1993), the result of a measurement depends "in a way not understood, on the choice of other quantum measurements,

that may possibly be performed". Mermin's 'proof' of the BKS theorem stated in terms of two-qubit observables can now be reformulated in terms of rays and maximal bases.

We shall employ a signature of the proofs in terms of the distance D_{ab} between two orthonormal bases a and b defined as (Planat, 2012)

$$D_{ab}^2 = 1 - \frac{1}{d-1} \sum_{i,j}^{d} \left(\left| \langle a_i | b_j \rangle \right|^2 - \frac{1}{d} \right)^2 . \tag{2}$$

The distance (2) vanishes when the bases are the same and is maximal (equal to unity) when the two bases a and b are mutually unbiased, $\left| \langle a_i | b_j \rangle \right|^2 = 1/d$, and only then. We shall see that the bases of a BKS proof employ a selected set of distances which happens to be a universal feature of the proof.

Using the list of the unnormalized eigenvectors (numbered consecutively)

$$\begin{array}{l} 1:[1000],\ \ 2:[0100],\ \ 3:[0010],\ \ 4:[0001],\ \ 5:[1111],\ \ 6:[11\bar{1}\bar{1}] \\ 7:[1\bar{1}1\bar{1}],\ \ 8:[1\bar{1}\bar{1}1],\ \ 9:[1\bar{1}\bar{1}\bar{1}],\ \ 10:[1\bar{1}11],\ \ 11:[11\bar{1}1],\ \ 12:[111\bar{1}] \\ 13:[1100],\ \ 14:[1\bar{1}00],\ \ 15:[0011],\ \ 16:[001\bar{1}],\ \ 17:[0101],\ \ 18:[010\bar{1}] \\ 19;[1010],\ \ 20:[10\bar{1}0],\ \ 21:[100\bar{1}],\ \ 22:[1001],\ \ 23:[01\bar{1}0],\ \ 24:[0110] \end{array} \tag{3}$$

one gets 24 complete orthogonal bases are as follows

$$\begin{array}{l} \mathbf{1}:\{1,2,3,4\},\ \mathbf{2}:\{5,6,7,8\},\ \mathbf{3}:\{9,10,11,12\},\ \mathbf{4}:\{13,14,15,16\}, \\ \mathbf{5}:\{17,18,19,20\},\ \mathbf{6}:\{21,22,23,24\},\ \mathbf{7}:\{1,2,15,16\},\ \mathbf{8}:\{1,3,17,18\}, \\ \mathbf{9}:\{1,4,23,24\},\ \mathbf{10}:\{2,3,21,22\},\ \mathbf{11}:\{2,4,19,20\},\ \mathbf{12}:\{3,4,13,14\}, \\ \mathbf{13}:\{5,6,14,16\},\ \mathbf{14}:\{5,7,18,20\},\ \mathbf{15}:\{5,8,21,23\},\ \mathbf{16}:\{6,7,22,24\}, \\ \mathbf{17}:\{6,8,17,19\},\ \mathbf{18}:\{7,8,13,15\},\ \mathbf{19}:\{9,10,13,16\},\ \mathbf{20}:\{9,11,18,19\}, \\ \mathbf{21}:\{9,12,22,23\},\ \mathbf{22}:\{10,11,21,24\},\ \mathbf{23}:\{10,12,17,20\},\ \mathbf{24}:\{11,12,14,15\}. \end{array} \tag{4}$$

Then, by normalizing rays, one obtains a finite set of distances between the 24 bases

$$\begin{aligned} D &= \{a_1, a_2, a_3, a_4, a_5\} = \{\sqrt{1/3}, \sqrt{7/12}, \sqrt{2/3}, \sqrt{5/6}, 1\} \\ &\approx \{0.58, 0.76, 0.82, 0.91, 1.000\}. \end{aligned}$$

Table 1 provides a histogram of distances for various parity proofs $v - l$.

The table reveals that there exist four main types of parity proofs arising from the 24 rays, that are of the type $18-9$, $20-11$, $22-13$ and $24-15$. Types $20-11$

Table 1 The histogram of distances for various parity proofs $v-l$ obtained from Mermin's square

Proof $v-l$	# Proofs	a_1	a_2	a_3	a_4	a_5
24-15	16	18	18	9	54	6
22-13A	96	12	18	3	42	3
22-13B	144	12	18	4	42	2
20-11A	96	6	18	0	30	1
20-11B	144	6	18	1	30	0
18-9	16	0	18	0	18	0

and $22-13$ subdivide into two non-isomorphic ones A and B as shown in Table 1 (Planat, 2012; Pavičić et al., 2005; Waegell and Aravind, 2011).

The 16 proofs of the $18-9$ type can be displayed as the 4×4 square (5) in which two adjacent proofs share three bases. Observe that each 2×2 square of adjacent proofs has the same shared base, which is taken as an index (e.g. the upper left-hand-side 2×2 square has index 7 and the lower right-hand-side square has index 10). All four indices in each row and in each column correspond to four disjoint bases that together partition the 24 rays.

$$
\begin{array}{cccc}
\begin{pmatrix} 7 & 8 & 10 \\ 13 & 14 & 16 \\ 22 & 23 & 24 \end{pmatrix}_{7} - \begin{pmatrix} 7 & 9 & 11 \\ 14 & 15 & 18 \\ 19 & 20 & 22 \end{pmatrix}_{20} - \begin{pmatrix} 8 & 9 & 12 \\ 16 & 17 & 18 \\ 20 & 21 & 24 \end{pmatrix}_{12} - \begin{pmatrix} 10 & 11 & 12 \\ 13 & 15 & 17 \\ 19 & 21 & 23 \end{pmatrix}_{23} - \\
\begin{pmatrix} 7 & 9 & 11 \\ 16 & 17 & 18 \\ 19 & 21 & 23 \end{pmatrix}_{17} - \begin{pmatrix} 7 & 8 & 10 \\ 13 & 15 & 17 \\ 20 & 21 & 24 \end{pmatrix}_{10} - \begin{pmatrix} 10 & 11 & 12 \\ 13 & 14 & 16 \\ 19 & 20 & 22 \end{pmatrix}_{14} - \begin{pmatrix} 8 & 9 & 12 \\ 14 & 15 & 18 \\ 22 & 23 & 24 \end{pmatrix}_{9} - \\
\begin{pmatrix} 8 & 9 & 12 \\ 13 & 15 & 17 \\ 19 & 20 & 22 \end{pmatrix}_{12} - \begin{pmatrix} 10 & 11 & 12 \\ 16 & 17 & 18 \\ 22 & 23 & 24 \end{pmatrix}_{23} - \begin{pmatrix} 7 & 8 & 10 \\ 14 & 15 & 18 \\ 19 & 21 & 23 \end{pmatrix}_{7} - \begin{pmatrix} 7 & 9 & 11 \\ 13 & 14 & 16 \\ 20 & 21 & 24 \end{pmatrix}_{20} - \\
\begin{pmatrix} 10 & 11 & 12 \\ 14 & 15 & 18 \\ 20 & 21 & 24 \end{pmatrix}_{14} - \begin{pmatrix} 8 & 9 & 12 \\ 13 & 14 & 16 \\ 19 & 21 & 23 \end{pmatrix}_{9} - \begin{pmatrix} 7 & 9 & 11 \\ 13 & 15 & 17 \\ 22 & 23 & 24 \end{pmatrix}_{17} - \begin{pmatrix} 7 & 8 & 10 \\ 16 & 17 & 18 \\ 19 & 20 & 22 \end{pmatrix}_{10} -
\end{array}
\tag{5}
$$

Diagrams for the proofs How can we account for the distance signature of a given proof? A simple diagram does the job.

The diagram for the $18-9$ proof is simply a 3×3 square. Below we give an explicit construction of the first proof that corresponds to the upper left-hand-side corner in (5). The 9 vertices of the graph are the 9 bases of the proof, the one-point crossing graph between the bases is the graph (6), with aut $= G_{72} = \mathbb{Z}_3^2 \rtimes D_4$. There

are 9 (distinct) edges that encode the 18 rays, a selected vertex/base of the graph is encoded by the union of the four edges/rays that are adjacent to it.

$$\begin{array}{ccccc}
\begin{pmatrix} 1 & 2 \\ 15 & 16 \end{pmatrix} & - 1 - & \begin{pmatrix} 1 & 3 \\ 17 & 18 \end{pmatrix} & - 3 - & \begin{pmatrix} 2 & 3 \\ 21 & 22 \end{pmatrix} \\
|_{16} & & |_{18} & & |_{22} \\
\begin{pmatrix} 5 & 6 \\ 14 & 16 \end{pmatrix} & - 5 - & \begin{pmatrix} 5 & 7 \\ 18 & 20 \end{pmatrix} & - 7 - & \begin{pmatrix} 6 & 7 \\ 22 & 24 \end{pmatrix} \\
|_{14} & & |_{20} & & |_{24} \\
\begin{pmatrix} 11 & 12 \\ 14 & 15 \end{pmatrix} & - 12 - & \begin{pmatrix} 10 & 12 \\ 17 & 20 \end{pmatrix} & - 10 - & \begin{pmatrix} 10 & 11 \\ 21 & 24 \end{pmatrix} \\
|_{15} & & |_{17} & & |_{21}
\end{array} - 2 - 6 - 11 \qquad (6)$$

As for the distances between the bases, two bases located in the same row (or the same column) have distance $a_2 = \sqrt{7/12}$, while two bases not in the same row (or column) have distance $a_4 = \sqrt{5/6} > a_2$, as readily discernible from Table 2 and the histogram in Table 1. Indeed, any proof of the $18 - 9$ type has the same diagram as (6).

Similar diagrams can be drawn to reflect the histogram of distances in proofs of a larger size. Below we restrict to the case of a $20 - 11A$ proof (where only the distance between two bases is made explicit, but not the common rays of the bases)

$$\begin{array}{ccccc}
\begin{pmatrix} 10 & 12 \\ 17 & 20 \end{pmatrix} & - a_2 - & \begin{pmatrix} 11 & 12 \\ 14 & 15 \end{pmatrix} & - a_2 - & \begin{pmatrix} 10 & 11 \\ 21 & 24 \end{pmatrix} \ldots a_4 = \sqrt{5/6} \ldots \\
|a_2 = \sqrt{7/12} & & |\, a_2 & & |a_2 \qquad \ldots \\
\begin{pmatrix} 1 & 3 \\ 17 & 18 \end{pmatrix} & - a_2 - & \begin{pmatrix} 1 & 2 \\ 15 & 16 \end{pmatrix} & - a_2 - & \begin{pmatrix} 1 & 4 \\ 23 & 24 \end{pmatrix} \ldots a_1 = \frac{1}{\sqrt{3}} \ldots \quad \begin{pmatrix} 1 & 2 \\ 3 & 4 \end{pmatrix} \\
|a_2 & & |a_2 & & |a_2 \qquad\qquad |a_5 = 1 \\
\begin{pmatrix} 5 & 7 \\ 18 & 20 \end{pmatrix} & - a_2 - & \begin{pmatrix} 5 & 6 \\ 14 & 16 \end{pmatrix} & - a_2 - & \begin{pmatrix} 5 & 8 \\ 21 & 23 \end{pmatrix} \ldots a_1 = \frac{1}{\sqrt{3}} \ldots \quad \begin{pmatrix} 5 & 6 \\ 7 & 8 \end{pmatrix} \\
|a_2 & & |a_2 & & |a_2 \qquad\qquad \ldots
\end{array} \qquad (7)$$

The proof consists of 11 bases, 9 of them have the same mutual diagram as in (6) and their mutual distance is $a_2 = \sqrt{7/12}$ (as shown) or $a_4 = \sqrt{5/6}$ (not shown), depending on whether they are located in the same row (or the same column) of the 3×3 square, or not. The extra two bases of the right-hand-side column are mutually unbiased (with distance $a_5 = 1$), their distance to any base of the same row is $1/\sqrt{3}$ and their distance to any base of the first row is a_4 (as shown).

3 Geometric Contextuality

Interpreting quantum theory is a long standing effort and not a single approach can exhaust all facets of this fascinating subject. Quantum information owes much to the concept of a (generalized) Pauli group for understanding quantum observables, their commutation, entanglement, contextuality and many other aspects, e.g. quantum

computing. Quite recently, it has been shown that quantum commutation relies on some finite geometries such as generalized polygons and polar spaces (Planat, 2011). Finite geometries connect to the classification of simple groups as understood by prominent researchers as Jacques Tits, Cohen Thas and many others (Planat and Zainuddin, 2017; Thas et al., 2004).

In the Atlas of finite group representations (Wilson et al., 2015), one starts with a free group G with relations, then the finite group under investigation P is the permutation representation of the cosets of a subgroup of finite index d of G (obtained thanks to the Todd-Coxeter algorithm). As a way of illustrating this topic, one can refer to (Planat and Zainuddin, 2017, Table 3) to observe that a certain subgroup of index 15 of the symplectic group $S_4'(2)$ corresponds to the $2QB$ (two-qubit) commutation of the 15 observables in terms of the generalized quadrangle of order two, denoted $GQ(2, 2)$ (alias the doily). For $3QB$, a subgroup of index 63 in the symplectic group $S_6(2)$ does the job and the commutation relies on the symplectic polar space $W_5(2)$ (Planat and Zainuddin, 2017, Table 7). An alternative way to approach $3QB$ commutation is in terms of the generalized hexagon $GH(2, 2)$ (or its dual) which occurs from a subgroup of index 63 in the unitary group $U_3(3)$ (Planat and Zainuddin, 2017, Table 8). Similar geometries can be defined for multiple qudits (instead of qubits).

The straightforward relationship of quantum commutation to the appropriate symmetries and finite groups was made possible thanks to techniques that we briefly summarize.

3.1 Finite Geometries from Cosets (Planat, 2015; Planat and Zainuddin, 2017; Planat et al., 2015)

Let H be a subgroup of index d of a free group G with generators and relations. A coset table over the subgroup H is built by means of a Coxeter-Todd algorithm. Given the coset table, on builds a permutation group P that is the image of G given by its action on the cosets of H. In this paper, the software Magma (Bosma, 2019) is used to perform these operations.

One needs to define the rank r of the permutation group P. First one asks that the d-letter group P acts faithfully and transitively on the set $\Omega = \{1, 2, \ldots, d\}$. The action of P on a pair of distinct elements of Ω is defined as $(\alpha, \beta)^p = (\alpha^p, \beta^p)$, $p \in P$, $\alpha \neq \beta$. The orbits of P on the product set $\Omega \times \Omega$ are called orbitals. The number of orbits is called the rank r of P on Ω. Such a rank of P is at least two, and it also known that two-transitive groups may be identified to rank two permutation groups.

One selects a pair $(\alpha, \beta) \in \Omega \times \Omega, \alpha \neq \beta$ and one introduces the two-point stabilizer subgroup $P_{(\alpha,\beta)} = \{p \in P | (\alpha, \beta)^p = (\alpha, \beta)\}$. There are $1 < m \leq r$ such non-isomorphic (two-point stabilizer) subgroups of P. Selecting one of them with $\alpha \neq \beta$, one defines a point/line incidence geometry $\mathcal{G}$ whose points are the elements of the

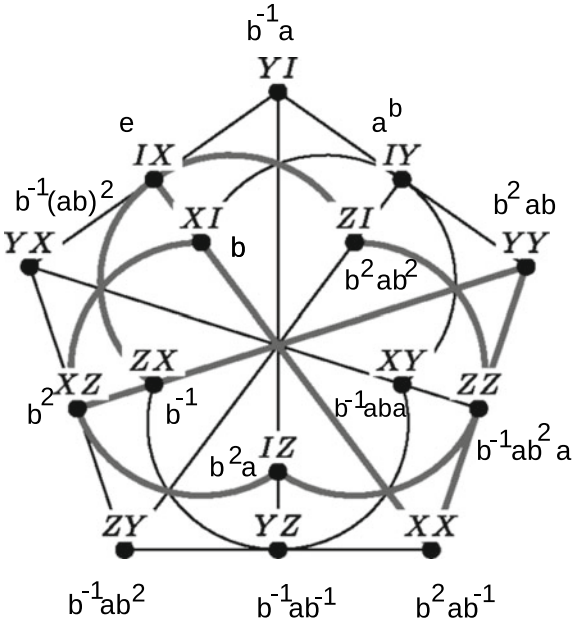

Fig. 1 The generalized quadrangle of order two $GQ(2, 2)$. The picture provides a representation in terms of the fifteen $2QB$ observables that are commuting by triples: the lines of the geometry. Bold lines are for an embedded 3×3 grid (also called Mermin square) that is a basic model of Kochen-Specker theorem (e.g. Planat and Zainuddin, 2017, Fig. 1 or (Planat, 2012)). The second representation is in terms of the cosets of the permutation group arising from the index 15 subgroup of $G \cong A_6$ (the 6-letter alternating group)

set Ω and whose lines are defined by the subsets of Ω that share the same two-point stabilizer subgroup. Two lines of $\mathcal{G}$ are distinguished by their (isomorphic) stabilizers acting on distinct subsets of Ω. A non-trivial geometry is obtained from P as soon as the rank of the representation $\mathcal{P}$ of P is $r > 2$, and at the same time, the number of non isomorphic two-point stabilizers of $\mathcal{P}$ is $m > 2$. Further, $\mathcal{G}$ is said to be *contextual* (shows *geometrical contextuality*) if at least one of its lines/edges is such that a set/pair of vertices is encoded by non-commuting cosets (Planat, 2015).

Figure 1 illustrates the application of the two-point stabilizer subgroup approach just described for the index 15 subgroup of the symplectic group is $S_4'(2) = A_6$ whose finite representation is
$H = \langle a, b | a^2 = b^4 = (ab)^5 = (ab^2)^5 = 1 \rangle$. The finite geometry organizing the coset representatives is the generalized quadrangle $GQ(2, 2)$. The other representation is in terms of the two-qubit Pauli operators, as first found in (Planat, 2011; Saniga and Planat, 2007). It is easy to check that all lines not passing through the coset e contains some mutually not commuting cosets so that the $GQ(2, 2)$ geometry is contextual. The embedded (3×3)-grid shown in bold (the so-called Mermin square) allows a $2QB$ proof of Kochen-Specker theorem (Planat, 2012).

3.2 *The Kochen-Specker Theorem with a Mermin Square of Two-Qubit Observables*

Let us show how to recover the geometry of the Mermin square, i.e. the (3×3) grid embedded in the generalized $GQ(2, 2)$ of Fig. 1. Recall that it is the basic model of two-qubit contextuality (Planat and Zainuddin, 2017, Fig. 1) (Planat, 2012). One starts with the free group $G = \langle a, b | b^2 \rangle$ and one makes use of the mathematical software Magma (Bosma, 2019). Then one derives the (unique) subgroup H of G that is of index nine and possesses a permutation representation P isomorphic to the finite group $\mathbb{Z}_3^2 \times \mathbb{Z}_2^2$ reflecting the symmetry of the grid. The permutation representation is as follows:

$$P = \langle 9 | (1, 2, 4, 8, 7, 3)(5, 9, 6), (2, 5)(3, 6)(4, 7)(8, 9) \rangle ,$$

where the list [1, ..., 9] means the list of coset representatives

$$[e, a, a^{-1}, a^2, ab, a^{-1}b, a^{-2}, a^3, aba].$$

The permutation representation P can be seen on a torus as in Fig. 2i.

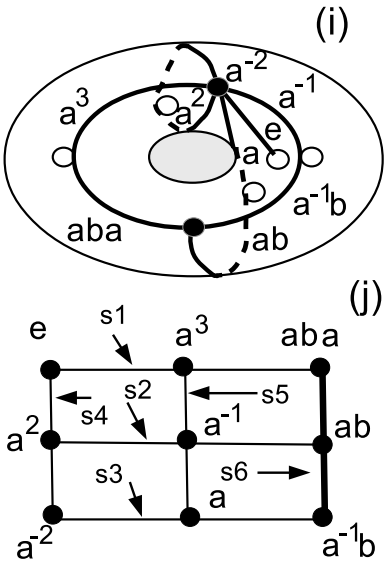

Fig. 2 The map (**i**) leading to Mermin's square (**j**). The two-point stabilizer subgroups of the permutation representation P corresponding to the dessin (one for each line) are as follows: $s_1 = (2, 3)(4, 7)(5, 6), s_2 = (1, 7)(2, 8)(6, 9), s_3 = (1, 4)(3, 8)(5, 9), s_4 = (2, 6)(3, 5)(8, 9), s_5 = (1, 9)(4, 5)(6, 7), s_6 = (1, 8)(2, 7)(3, 4)$, where the points of the square (resp. the edges of the dessin d'enfant) are labeled as $[1, .., 9] = [e, a, a^{-1}, a^2, ab, a^{-1}b, a^{-2}, a^3, aba]$

Next, we apply the procedure described at the top of this subsection. There are two types of two-point stabilizer subgroups isomorphic to the single element group $\mathbb{Z}_1$ or to the two-element group $\mathbb{Z}_2$. Both define the geometry of a (3×3) grid comprising six lines identified, by their non-identical, but isomorphic two-point stabilizers s_1 to s_6, made explicit in the caption of Fig. 2. The first grid (not shown) is considered non-contextual in the sense that the cosets on a line are commuting. The second grid, shown in Fig. 2j, is contextual in the sense that the right column does not have all its triples of cosets mutually commuting. The non-commuting cosets on this line reflect the contextuality that occurs when one takes two-qubit coordinates for the points of the grid, see (Planat, 2015) for more details about the relationship between non-commuting cosets and geometric contextuality.

4 Exotic Contextuality

We already approached the topic of quantum contextuality (QC) in two ways. In Sect. 2, we found how the 3×3 grid (or Mermin square) can be considered as a building block of QC by proving the BKS theorem, either at level of two-qubit operators that parametrize the grid or at the level of rays that correspond to eigenstates attached to the operators of the grid. In Sect. 3, a group theoretical language with two-letter words was found to nicely mimic QC in the Mermin square and its embedding generalized quadrangle $GQ(2, 2)$—the locus of of the two-qubit Pauli group. In such an approach, geometric contextuality corresponds to QC. Now, we jump to a possible interpretation of this language by seeing the QC-geometries as creatures of exotic four-manifolds that one may identify to our familiar space-time (Planat, 2020).

We introduce the concept of exotic contextuality for such an interpretation. Moreover, such a type of contextuality is related to a model of quantum computing based on magic states that we developed in a series of papers (Planat and Gedik, 2017; Planat et al., 2018, 2019). In quantum information theory, the two-qubit configuration and its properties: quantum entanglement and quantum contextuality have been discussed at length as prototypes of peculiarities or resources in the quantum world. Our Sect. 3.2 mainly featured the quantum contextuality of two-qubit systems. Our model of quantum computing is based on the concept of a magic state—a state that has to be added to the eigenstates of the d-dimensional Pauli group- in order to allow universal quantum computation. This was started by Bravyi & Kitaev in 2005 (Bravyi and Kitaev, 2005) for qubits ($d = 2$). A subset of magic states consists of states associated to minimal informationally complete measurements, that we called MIC states (Planat and Gedik, 2017). We require that magic states should be MIC states as well. For getting the candidate MIC states, one uses the fact that a permutation may be realized as a permutation matrix/gate and that mutually commuting matrices share eigenstates. They are either of the stabilizer type (as elements of the Pauli group) or of the magic type. One keeps magic states that are MIC states in order to preserve a complete information during the computation and measurements.

A further step in our quantum computing model was to introduce a 3-dimensional manifold M^3 whose fundamental group $G = \pi_1(M^3)$ would be the source of MIC states (Planat et al., 2018, 2019). Recall that G is a free group with relations and that a d-dimensional MIC state may be obtained from the permutation group that organizes the cosets of an appropriate subgroup of index d of G.

It was considered by us quite remarkable that two group geometrical axioms very often govern the MIC states of interest (Planat et al., 2019), viz (i) the normal (or conjugate) closure $\{g^{-1}hg|g \in G \text{ and } h \in H\}$ of the appropriate subgroup H of G equals G itself and (ii) there is no geometry (a triple of cosets do not produce equal pairwise stabilizer subgroups). See (Planat et al., 2019, Sect. 1.1) for our method of building a finite geometry from coset classes. But these rules had to be modified by allowing either the simultaneous falsification of (i) and (ii) or by tolerating a few exceptions. If it happens that (ii) is violated, one gets geometric contextuality, the parallel to quantum contextuality (Planat, 2015) that one featured in Sect. 3.

It is known that there exist infinitely many 4-manifolds that are homeomorphic but non diffeomorphic to each other (Akbulut, 1991a, 2016; Gompf and Stipsicz, 1999; Scorpian, 2011). They can be seen as distinct copies of space-time not identifiable to the ordinary Euclidean space-time. A cornerstone of our approach is an 'exotic' 4-manifold called an Akbulut cork W that is contractible, compact and smooth, but not diffeomorphic to the 4-ball (Akbulut, 1991a). In our approach, we do not need the full toolkit of 4-manifolds since we are focusing on W and its neighboors only. All what we need is to understand the handlebody decomposition of a 4-manifold, the fundamental group $\pi_1(\partial W)$ of the 3-dimensional boundary ∂W of W, and related fundamental groups. Following the methodology of our previous work (Planat and Gedik, 2017; Planat et al., 2018), the subgroup structure of such π_1's corresponds to the Hilbert spaces of interest. Our view is close to the many-worlds interpretation of quantum mechanics where all possible outcomes of quantum measurements are realized in some 'world' and are objectively real (DeWitt, 1970). One arrives at a many-manifolds view of quantum computing -reminiscent of the many-worlds- where the many-manifolds are in an exotic class and can be seen as many-quantum generalized measurements, the latter being POVM's (positive operator valued measures).

4.1 Excerpts on the Theory of 4*-manifolds and Exotic* R^4*'s*

Handlebody of a 4-manifold. Let us introduce some excerpts of the theory of 4-manifolds needed for our paper (Akbulut, 2016; Gompf and Stipsicz, 1999; Scorpian, 2011). It concerns the decomposition of a 4-manifold into one- and two-dimensional handles as shown in Fig. 3 (Akbulut, 2016, Figs. 1.1 and 1.2). Let B^n and S^n be the n-dimensional ball and the n-dimensional sphere, respectively. An observer is placed at the boundary $\partial B^4 = S^3$ of the 0-handle B^4 and watch the attaching regions of the 1- and 2-handles. The attaching region of 1-handle is a pair of balls B^3 (the yellow balls), and the attaching region of 2-handles is a framed knot (the red knotted circle) or a knot going over the 1-handle (shown in blue). Notice that the 2-handles are

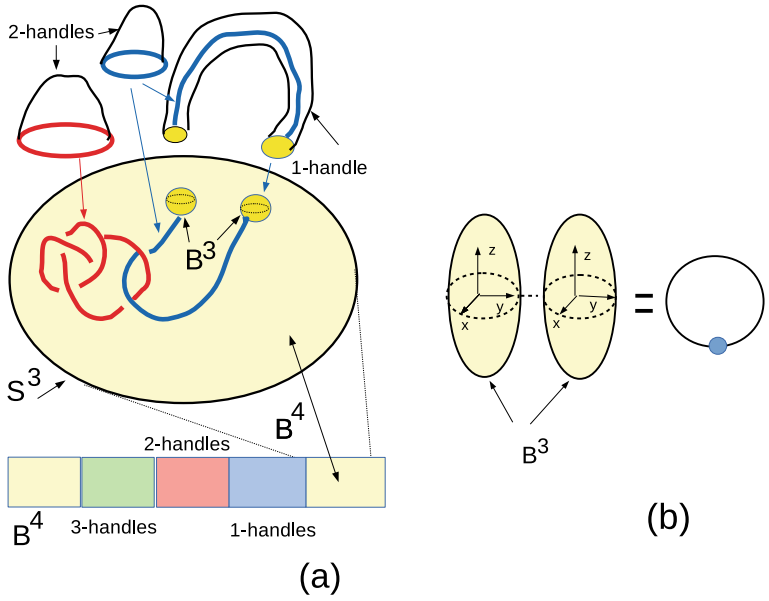

Fig. 3 **a** Handlebody of a 4-manifold with the structure of 1- and 2-handles over the 0-handle B^4, **b** the structure of a 1-handle as a dotted circle $S^1 \times B^3$

attached after the 1-handles. For closed 4-manifolds, there is no need of visualizing a 3-handle since it can be directly attached to the 0-handle. The 1-handle can also be figured out as a dotted circle $S^1 \times B^3$ obtained by squeezing together the two three-dimensional balls B^3 so that they become flat and close together (Gompf and Stipsicz, 1999, p. 169) as shown in Fig. 3b. For the attaching region of a 2- and a 3-handle one needs to enrich our knowledge by introducing the concept of an Akbulut cork to be described later on. The surgering of a 2-handle to a 1-handle is illustrated in Fig. 4a (see also Gompf and Stipsicz, 1999, Fig. 5.33). The 0-framed 2-handle (left) and the 'dotted' 1-handle (right) are diffeomorphic at their boundary ∂. The boundary of a 2- and a 3-handle is intimately related to the Akbulut cork shown in Fig. 4b as described at the Sect. 4.1.

Akbulut cork. A Mazur manifold is a contractible, compact, smooth 4-manifold (with boundary) not diffeomorphic to the standard 4-ball B^4 (Akbulut, 2016). Its boundary is a homology 3-sphere. If one restricts to Mazur manifolds that have a handle decomposition into a single 0-handle, a single 1-handle and a single 2-handle then the manifold has to be of the form of the dotted circle $S^1 \times B^3$ (as in Fig. 4a) (right) union a 2-handle.

Recall that, given p, q, r (with $p \leq q \leq r$), the Brieskorn 3-manifold $\Sigma(p, q, r)$ is the intersection in the complex 3-space $\mathbb{C}^3$ of the 5-dimensional sphere S^5 with the surface of equation $z_1^p + z_2^q + z_3^r = 0$. The smallest known Mazur manifold is the Akbulut cork W (Akbulut, 1991a, b) pictured in Fig. 4b and its boundary is the Brieskorn homology sphere $\Sigma(2, 5, 7)$.

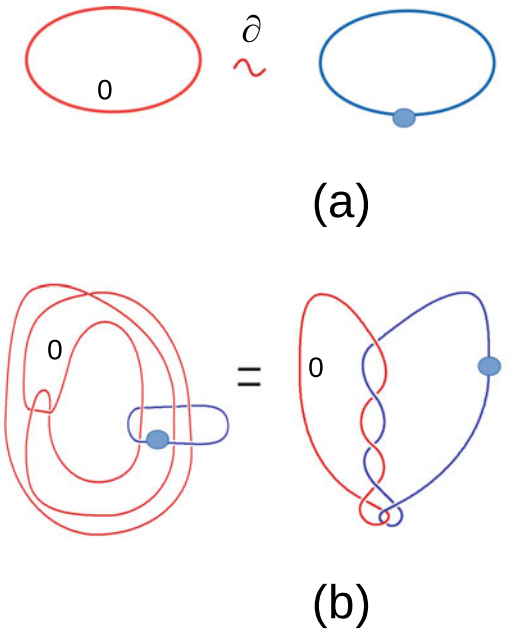

Fig. 4 **a** A 0-framed 2-handle $S^2 \times B^2$ (left) and a dotted 1-handle $S^1 \times B^3$ (right) are diffeomorphic at their boundary $\partial = S^2 \times S^1$, **b** two equivalent pictures of the Akbulut cork W

According to Akbulut and Durusoy (2005), there exists an involution $f : \partial W \to \partial W$ that surgers the dotted 1-handle $S^1 \times B^3$ to the 0-framed 2-handle $S^2 \times B^2$ and back, in the interior of W. Akbulut cork is shown in Fig. 4b. The Akbulut cork has a simple definition in terms of the framings ± 1 of $(-3, 3, -3)$ pretzel knot also called $K = 9_{46}$ (Akbulut and Durusoy, 2005, Fig. 3). It has been shown that $\partial W = \Sigma(2, 5, 7) = K(1, 1)$ and $W = K(-1, 1)$.

Exotic manifold R^4. An exotic R^4 is a differentiable manifold that is homeomorphic but not diffeomorphic to the Euclidean space $\mathbb{R}^4$. An exotic R^4 is called small if it can be smoothly embedded as an open subset of the standard $\mathbb{R}^4$ and is called large otherwise. Here we are concerned with an example of a small exotic R^4. Let us quote Theorem 1 of (Akbulut, 1991a).

There is a smooth contractible 4-manifold V with $\partial V = \partial W$, such that V is homeomorphic but not diffeomorphic to W relative to the boundary.

Sketch of proof (Akbulut, 1991a):

Let α be a loop in ∂W as in Fig. 5a. α is not slice in W (does not bound an imbedded smooth B^2 in W) but $\phi(\alpha)$ is slice. Then ϕ does not extend to a self-diffeomorphism $\phi : W \to W$.

It is time to recall that a cobordism between two oriented m-manifolds M and N is any oriented $(m + 1)$-manifold W_0 such that the boundary is $\partial W_0 = \bar{M} \cup N$, where M appears with the reverse orientation. The cobordism $M \times [0, 1]$ is called the trivial cobordism. Next, a cobordism W_0 between M and N is called an h-cobordism if W_0 is

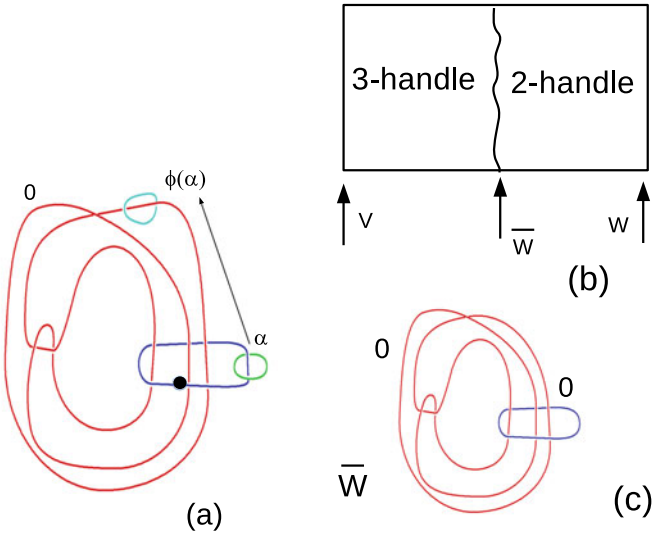

Fig. 5 **a** The loop α is not slice on the Akbulut cork, **b** the non-trivial h-cobordism between small exotic manifolds V and W, **c** the mediating 4-manifold $\bar{W}$

homotopically like the trivial cobordism. The h-cobordism due to S. Smale in 1960, states that if M^m and N^m are compact simply-connected oriented M-manifolds that are h-cobordant through the simply-connected $(m+1)$-manifold W_0^{m+1}, then M and N are diffeomorphic (Scorpian, 2011, p. 29). But this theorem fails in dimension 4. If M and N are cobordant 4-manifolds, then N can be obtained from M by cutting out a compact contractible submanifold W and gluing it back in by using an involution of ∂W. The 4-manifold W is a 'fake' version of the 4-ball B^4 called an Akbulut cork (Scorpian, 2011, Fig. 2.23).

The h-cobordism under question in our example may be described by attaching an algebraic cancelling pair of 2- and 3-handles to the interior of Akbulut cork W as pictured in Fig. 5b (see Akbulut, 1991a, p. 343). The 4-manifold $\bar{W}$ mediating V and W is as shown in Fig. 5c [alias the 0-surgery $L7a6(0,1)(0,1)$] (see Akbulut, 1991a, p. 355).

Following (Akbulut, 1991b), the result is relative since V itself is diffeomorphic to W but such a diffeomorphism cannot extend to the identity map $\partial V \to \partial W$ on the boundary. In (Akbulut, 1991b), two exotic manifolds Q_1 and Q_2 are built that are homeomorphic but not diffeomorphic to each other in their interior.

By the way, the exotic R^4 manifolds Q_1 and Q_2 are related by a diffeomorphism $Q_1 \# S^2 \times S^2 \approx Q \approx Q_2 \# S^2 \times S^2$ (where # is the connected sum between two manifolds) and Q is called the middle level between such connected sums. This is shown in Fig. 6 for the two R^4 manifolds Q_1 and Q_2 (Akbulut, 1991b), (Gompf, 1993, Fig. 2).

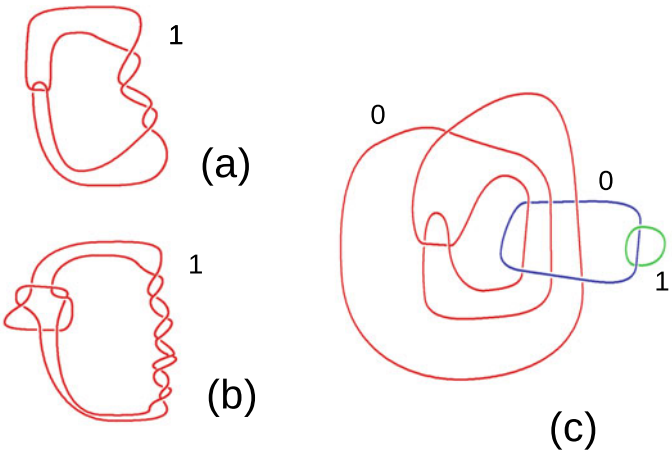

Fig. 6 Exotic R^4 manifolds Q_1 shown in (**a**) and Q_2 shown in (**b**). The connected sums $Q_1\#S^2 \times S^2$ and $Q_2\#S^2 \times S^2$ are diffeomorphic with middle level Q shown in (**c**)

4.2 Finite Geometry of Small Exotic R^4's, Quantum Computing and Quantum Contextuality

In the present paper, we choose G as the fundamental group $\pi_1(M^4)$ of a 4-manifold M^4 that is the boundary ∂W of Akbulut cork W, or governs the Akbulut h-cobordism. More precisely, one takes the manifold M^4 as $\bar{W}$ in Fig. 5 and Q in Fig. 6. Manifolds Q_1 and Q_2 are the small exotic R^4's of Ref. (Akbulut, 1991b, Figs. 1 and 2). There are homeomorphic but not diffeomorphic to each other in their interiors. This choice has two important consequences.

In the present paper, we choose G as the fundamental group $\pi_1(M^4)$ of a 4-manifold M^4 that is the boundary ∂W of Akbulut cork W, or governs the Akbulut h-cobordism. More precisely, one takes the manifold M^4 as $\bar{W}$ in Fig. 5 and Q in Fig. 6. Manifolds Q_1 and Q_2 are the small exotic R^4's of Ref. (Akbulut, 1991b, Figs. 1 and 2). There are homeomorphic but not diffeomorphic to each other in their interiors. This choice has two important consequences.

Recall the introduction of this section that that axioms (i) and (ii) are expected to govern the subgroup structure of groups G relevant to our model of quantum computing based on magic states. For the aforementioned manifolds M^4, the fundamental group $G = \pi_1(M^4)$ is such that (i) is always satisfied and that (ii) most often is true or geometric contextuality occurs with corresponding finite geometries of great interest such as the Fano plane $PG(2, 2)$ (at index 7), the Mermin's pentagram (at index 10), the finite projective space $PG(3, 2)$ or its subgeometry $GQ(2, 2)$ -known to control 2-qubit commutation (Planat et al., 2019, Fig. 1) (at index 15), the Grassmannian Gr(2, 8) -containing Cayley-Dickson algebras (at index 28) and a few maximally multipartite graphs.

Second, this new frame of 'exotic contextuality' provides a physical interpretation of quantum computation and measurements as follows. Let us imagine that $\mathbb{R}^4$ is our familiar space-time. Thus the 'fake' 4-ball W -the Akbulut cork- allows the existence of smoothly embedded open subsets of space-time -the exotic R^4 manifolds such as Q_1 and Q_2- that we interpret in this model as 4-manifolds associated to quantum measurements.

The boundary ∂W of Akbulut cork. As announced earlier $\partial W = K(1, 1) \equiv \Sigma(2, 5, 7)$ is a **Brieskorn sphere** with fundamental group

$$\pi_1(\Sigma(2, 5, 7)) = \langle a, b | aBab^2aBab^3, a^4bAb \rangle, \text{ where } A = a^{-1}, B = b^{-1}.$$

The cardinality structure of subgroups of this fundamental group is found to be the sequence

$$\eta_d[\pi_1(\Sigma(2, 5, 7))] = [0, 0, 0, 0, 0, \ 0, 2, 1, 0, 3, \ 0, 0, 0, \mathbf{12}, \mathbf{145}, \ \mathbf{178}, 47, 0, 0, \mathbf{4}, \cdots].$$

All the subgroups H of the above list satisfy axiom (i).

Up to index 28, exceptions to axiom (ii) can be found at index $d = 14, 16, 20$ featuring the geometry of multipartite graphs $K_2^{(d/2)}$ with $d/2$ parties, at index $d = 15$ and finally at index 28. Here and below the bold notation features the existence of such exceptions.

Apart from these exceptions, the permutation group organizing the cosets is an alternating group A_d. The coset graph is the complete graph K_d on d vertices. One cannot find a triple of cosets with strictly equal pairwise stabilizer subgroups of A_d (no geometry), thus (ii) is satisfied.

At index 15, when (ii) is not satisfied, the permutation group organizing the cosets is isomorphic to A_7. The stabilized geometry is the finite projective space $PG(3, 2)$ (with 15 points, 15 planes and 35 lines) as illustrated in Fig. 7a. The geometry is contextual in the sense that all lines not going through the identity element do not show mutually commuting cosets.

At index 28, when (ii) is not satisfied, there are two cases. In the first case, the group P is of order 2^8 8! and the geometry is the multipartite graph $K_4^{(7)}$. In the second case, the permutation group is $P = A_8$ and the geometry is the configuration $[28_6, 56_3]$ on 28 points and 56 lines of size 3. In (Saniga, 2015), it was shown that the geometry in question corresponds to the combinatorial Grassmannian of type Gr(2, 8), alias the configuration obtained from the points off the hyperbolic quadric $Q^+(5, 2)$ in the complex projective space $PG(5, 2)$. Interestingly, Gr(2, 8) can be nested by gradual removal of a so-called 'Conwell heptad' and be identified to the tail of the sequence of Cayley-Dickson algebras (Saniga, 2015; Saniga et al., 2015, Table 4).

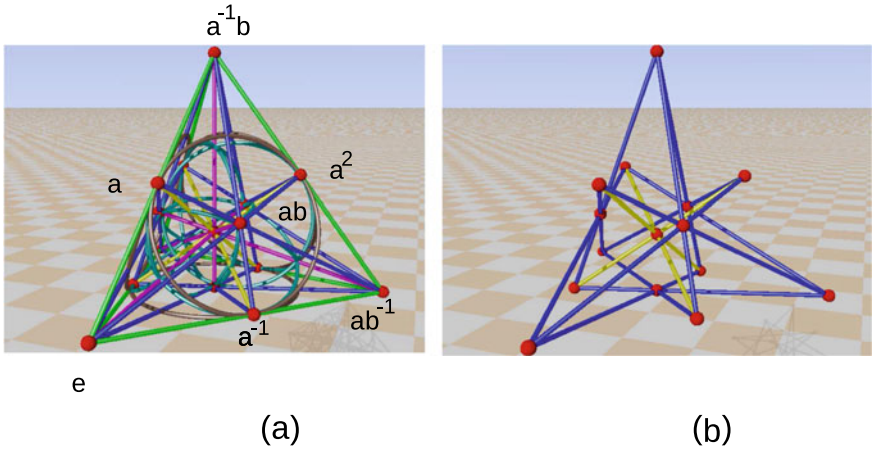

Fig. 7 **a** A picture of the smallest finite projective space $PG(3, 2)$. It is found at Frans Marcelis website (Marcelis, 2020). The coset coordinates are for a Fano plane $PG(2, 2)$ of $PG(3, 2)$. **b** A picture of the generalized quadrangle of order two $GQ(2, 2)$ embedded in $PG(3, 2)$. It may also be found at Frans Marcelis website

One expects a connection of the 28-point configuration to a del Pezzo surface of degree 2 (since the 56 lines of such a del Pezzo surface map in pairs to the 28 bitangents of a quartic).

The $[28_6, 56_3]$ *configuration*. Below are given some hints about the configuration that is stabilized at the index 28 subgroup H of the fundamental group $\pi_1(\partial W)$ whose permutation group P organizing the cosets is isomorphic to A_8. Recall that ∂W is the boundary of Akbulut cork W. The 28-letter permutation group P has two generators as follows

$$P = \langle 28|g_1, g_2\rangle \quad with \quad g_1 = (2, 4, 8, 6, 3)(5, 10, 15, 13, 9)(11, 12, 18, 25, 17)$$
$$(14, 20, 19, 24, 21)(16, 22, 26, 28, 23), \quad g_2 = (1, 2, 5, 11, 6, 7, 3)(4, 8, 12, 19, 22, 14, 9)$$
$$(10, 16, 24, 27, 21, 26, 17)(13, 20, 18, 25, 28, 23, 15).$$

Using the method described in Sect. 3.1, one derives the configuration $[28_6, 56_3]$ on 28 points and 56 lines. As shown in [Table 4] (Saniga, 2015), the configuration is isomorphic to the combinatorial Grassmannian Gr(2, 8) and nested by a sequence of binomial configurations isomorphic to Gr$(2, i)$, $i \leq 8$, associated with Cayley-Dickson algebras. This statement is checked by listing the 56 lines on the 28 points of the configuration as follows

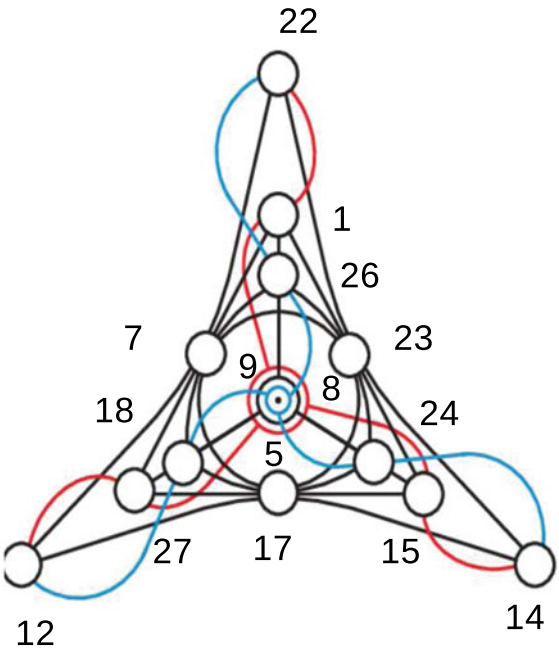

Fig. 8 The Cayley-Salmon configuration built around the Desargues configuration (itself built around the Pasch configuration) as in (Saniga et al., 2015, Fig. 12)

{1, 7, 27}, → **Gr**(**2**, **3**)

{1, 15, 23}, {15, 17, 27}, {7, 17, 23}, → **Gr**(**2**, **4**)

{1, 5, 26}, {5, 18, 27}, {5, 15, 24}, {23, 24, 26}, {17, 18, 24}, {7, 18, 26}, → **Gr**(**2**, **5**)

{12, 14, 17}, {1, 9, 22}, {5, 8, 9}, {9, 14, 15}, {7, 12, 22}, {8, 12, 18},

{8, 14, 24}, {8, 22, 26}, {14, 22, 23}, {9, 12, 27}, → **Gr**(**2**, **6**)

{3, 10, 15}, {3, 6, 24}, {3, 17, 25}, {3, 23, 28}, {1, 10, 28}, {3, 14, 19}, {7, 25, 28}, {6, 8, 19},

{19, 22, 28}, {5, 6, 10}, {12, 19, 25}, {10, 25, 27}, {9, 10, 19}, {6, 18, 25}, {6, 26, 28}, → **Gr**(**2**, **7**)

{4, 11, 12}, {11, 21, 25}, {6, 20, 21}, {2, 3, 21}, {2, 4, 14}, {7, 11, 16}, {2, 16, 23}, {1, 13, 16},

{2, 11, 17}, {4, 19, 21}, {16, 20, 26}, {2, 13, 15}, {11, 13, 27}, {16, 21, 28}, {2, 20, 24},

{5, 13, 20}, {11, 18, 20}, {4, 9, 13}, {4, 8, 20}, {4, 16, 22}, {10, 13, 21} → **Gr**(**2**, **8**).

More precisely, the distinguished configuration $[21_5, 35_3]$ isomorphic to Gr(2, 7) in the list above is stabilized thanks to the subgroup of P isomorphic to A_7. The distinguished Cayley-Salmon configuration $[15_4, 20_3]$ isomorphic to Gr(2, 6) in the list is obtained thanks to one of the two subgroups of P isomorphic to A_6. The upper stages of the list correspond to a Desargues configuration $[10_3, 10_3]$, to a Pasch configuration $[6_2, 4_3]$ and to a single line$[3_1, 1_3]$ and are isomorphic to the Grassmannians Gr(2, 5), Gr(2, 4) and Gr(2, 3), respectively. The Cayley-Salmon configuration configuration is shown on Fig. 8, see also (Saniga et al., 2015, Fig. 12).

For the embedding of Cayley-Salmon configuration into $[21_5, 35_3]$ configuration, see (Saniga et al., 2015, Fig. 18).

Frank Marcelis provides a parametrization of the Cayley-Salmon configuration in terms of 3-qubit operators (Marcelis, 2020).

Not surprisingly, geometric contextuality (in the coset coordinatization not given here) is a common feature of all lines except for the ones going through the identity element.

As a final note for this subsection, we found Brieskorn spheres other than $\Sigma(2, 5, 7)$ whose fundamental group admits an index 28 subgroup isomorphic to A_8 whose geometry is the configuration with 28 points and 56 lines. Three-manifolds $\Sigma(3, 4, 5)$, $\Sigma(3, 4, 7)$ and $\Sigma(3, 5, 7)$ are such Brieskorn spheres.

5 Conclusion

To conclude, it has been shown that the group theoretical language seems efficient for describing quantum reality. We introduced the concepts of geometric and exotic contextuality for quantum theory and quantum measurements. In other papers dealing with slightly different subjects, we found that 'informationally complete' magic states may be defined as irreducible characters of an appropriate finite group. These characters are useful in the context of quark and lepton mixings (Planat et al., 2020a) and in the context of the universal code of life—the genetic code (Planat et al., 2020b, 2021). What next? Proteins are the language of life. We have much to learn about quantum mechanics by decoding its 20-letter language, e.g.

$MGFTCPNSDCLYSRSEWSNRALREEGLSFSMRCPGACCGAML V \cdots$, is the beginning of the sentence of spike protein of SARS-Cov-2. Understanding the contextuality of life is the next step of this type of research.

References

Akbulut, S. (2016). *4-manifolds, Oxford graduate texts in mathematics* (Vol. 25). Oxford University Press.

Akbulut, S., & Durusoy, S. (2005). An involution acting nontrivially on Heegard-Floer homology. In *Geometry and topology of manifolds* (Fields Inst. Commun., Amer. Math. Soc., Providence, Rhode Island), (Vol. 47, pp. 1–9).

Akbulut, S. (1991). A fake compact contractible 4-manifold. *Journal of Differential Geometry, 33,* 335–356.

Akbulut, S. (1991). An exotic 4-manifold. *Journal of Differential Geometry, 33,* 357–361.

Bohr, N. Philosophy of Science Vol. 37 (1934), p. 157, and in The Truth of Science : Physical Theories and Reality (1997) by Roger Gerhard Newton, p. 176.

Bosma, W., Cannon, J. J., Fieker, C., & Steel, A. (Eds.), *Handbook of Magma functions*, Edition 2.23 (2017), 5914pp. Accessed on January 1, 2019.

Bravyi, S., & Kitaev, A. (2005). Universal quantum computation with ideal Clifford gates and noisy ancillas. *Physical Review A,71*, 022316.

Cabello, A., Estebaranz, J. M., & Garcia-Alcaine, G. (1996). *Physics Letters A, 212,* 183.
DeWitt, B. S. (1970). Quantum mechanics and reality. *Physics Today, 23,* 30.
Esfeld, M. (1999). Quantum holism and the philosophy of mind. *Journal of Consciousness Studies, 6,* 23–28.
Ferrero, M., Salgado, D., & Sánchez-Gómez, J. L. (2004). Is the epistemic view of quantum mechanics incomplete? *Foundations of Physics, 34,* 1993–2003.
Gompf, R. E. (1993). An exotic menagerie, *37*, 199–223.
Gompf, R. E., & Stipsicz, A. I. (1999). *4-manifolds and Kirby calculus*, Graduate Studies in Mathematics (Vol. 20). American Mathematical Society.
Marcelis, F. (2020). https://fgmarcelis.wordpress.com/pg32/pg32-1/ and https://fgmarcelis.wordpress.com/mermin-cayley-salmon-desargues. Accessed on January 1, 2020.
Mermin, N. D. (1993). Hidden variables and the two theorems of John Bell Rev. *Modern of Physics, 65,* 803–815.
Miller, E. (2014). Quantum entanglement, Bohmian mechanics, an humean supervenience. *Australasian Journal of Philosophy, 92,* 567–83.
Pavičić, M., Merlet, J.-P., McKay, B. D., & Megill, N. D. (2005). Kochen-Specker vectors. *Journal of Physics A: Mathematical Generation,38*, 1577–1592.
Peres, A. (1993). *Quantum theory, concepts and methods*. Dordrecht: Kluwer.
Planat, M. (2011). Pauli graphs when the Hilbert space dimension contains a square: Why the Dedekind psi function? *Journal Physics A Mathematical Theoretical44*, 045301.
Planat, M., & Gedik, Z. (2017). Magic informationally complete POVMs with permutations. *Royal Society Open Science,4*, 170387.
Planat, M., Giorgetti, A., Holweck, F., & Saniga, M. (2015). Quantum contextual finite geometries from dessins d'enfants. *International Journal of Geometric Methods in Modern Physics,12*, 1550067.
Planat, M. (2012). On small proofs of the Bell-Kochen-Specker theorem for two, three and four qubits. *The European Physical Journal Plus, 127,* 86.
Planat, M. (2015). Geometry of contextuality from Grothendieck's Coset space. *Quantum Information Processing, 14,* 2563–2575.
Planat, M. (2016). Two-letter words and a fundamental homomorphism ruling geometric contextuality. *Symmetry, Culture and Science, 1,* 1–16.
Planat, M. (2020). Quantum computation and measurements from an exotic space-time R^4. *Symmetry, 12,* 736.
Planat, M., Aschheim, R., Amaral, M. M., Fang, F., & Irwin, K. (2020). Complete quantum information in the DNA genetic code. *Symmetry, 12,* 1993.
Planat, M., Aschheim, R., Amaral, M. M., & Irwin, K. (2018). Universal quantum computing and three-manifolds. *Symmetry, 10,* 773.
Planat, M., Aschheim, R., Amaral, M. M., & Irwin, K. (2019). Group geometrical axioms for magic states of quantum computing. *Mathematics, 7,* 948.
Planat, M., Aschheim, R., Amaral, M. M., & Irwin, K. (2020). Informationally complete characters for quark and lepton mixings. *Symmetry, 12,* 1000.
Planat, M., Chester, D., Aschheim, R., Amaral, M. M., Fang, F., & Irwin, K. (2021). Finite groups for the Kummer surface: The genetic code and quantum gravity. *Quantum Reports, 3,* 68–79.
Planat, M., & Zainuddin, H. (2017). Zoology of Atlas-Groups: Dessins D'enfants, finite geometries and quantum commutation. *Mathematics (MDPI), 5,* 6.
Quantum contextuality, https://en.wikipedia.org/wiki/Quantum_contextuality. Accessed on January 15, 2021.
Saniga, M. (2015). The complement of binary Klein quadric as a combinatoriam Grassmannian. *Mathematics, 3,* 481–486.
Saniga, M., Holweck, F., & Pracna, P. (2015). From Cayley-Dickson algebras to combinatorial Grassmannians. *Mathematics, 3,* 1192–1221.
Saniga, M., & Planat, M. (2007). Multiple qubits as symplectic polar spaces of order two. *Advanced Studies in Theoretical Physics, 1,* 1.

Scorpian, A. (2011). *The wild world of 4-manifolds*. American Mathematical Society.

Thas, J., & van Maldeghem, H. (2004).Generalized polygons in finite projective spaces. In *Distance-Regular Graphs and Finite Geometry, in Special Issue: Conference on Association Schemes, Codes and Designs, Proceedings of the 2004 Workshop on Distance-regular Graphs and Finite Geometry (Com 2 MaC 2004)*, Busan, Korea, 19–23 July 2004.

Waegell, M., & Aravind, P. K. (2011). Parity proofs of the Kochen-Specker Theorem Basedon the 24 Rays of Peres, *Foundation of Physics,41* 1786–99.

Wilson, R., Walsh, P., Tripp, J., Suleiman, I., Parker, R., Norton, S., Nickerson, S., Linton, S., Bray, J., & Abbott, R. (2015). *ATLAS of finite group representations, Version 3*. Available online: http://brauer.maths.qmul.ac.uk/Atlas/v3/exc/TF42/. Accessed on June 2015.